JOURNAL OF CATALYSIS 139, 490–503 (1993)

Infrared Studies of the Interactions of C_2H_4 and H_2 with $Rh^+(CO)_2$ and CO Adsorbed on $RhCl_3/SiO_2$ and $Rh(NO_3)_3/SiO_2$

STEVEN S. C. CHUANG,[1] GIRISH SRINIVAS, AND ANANYA MUKHERJEE

Department of Chemical Engineering, The University of Akron, Akron, Ohio 44325

Received August 23, 1991; revised September 17, 1992

Interactions of C_2H_4/H_2 with $Rh^+(CO)_2/SiO_2$ and CO adsorbed on $RhCl_3/SiO_2$ and $Rh(NO_3)_3/SiO_2$ and the activity of these catalysts for ethylene hydroformylation have been studied by infrared spectroscopy. Chemisorption of CO on $RhCl_3/SiO_2$ and $Rh(NO_3)_3/SiO_2$ at 298 K results in the formation of linear CO on Rh^+ (or Rh^{+2}) and Rh^{+3} sites as well as gem-dicarbonyl. Temperature-programmed decomposition studies show that thermal stability of these adsorbed CO species decreases in the following order: linear CO on Rh^+ of $RhCl_3/SiO_2$ > $Rh^+(CO)_2$ on $Rh(NO_3)_3/SiO_2$ > $Rh^+(CO)_2$ and linear CO on Rh^{+3} on $RhCl_3/SiO_2$. Linear CO on Rh^+ sites is more active than $Rh^+(CO)_2$ on either $Rh(NO_3)_3/SiO_2$ or $RhCl_3/SiO_2$ at 298 K toward C_2H_4 and H_2 leading to the formation of propionaldehyde. Gem-dicarbonyl is observed as a dominant CO species adsorbed on $RhCl_3/SiO_2$ while both gem-dicarbonyl and linear CO on Rh^0 sites are found on $Rh(NO_3)_3/SiO_2$ during ethylene hydroformylation at 393 K and 1 MPa. $RhCl_3/SiO_2$ shows higher hydroformylation selectivity than $Rh(NO_3)_3/SiO_2$. $RhCl_3/SiO_2$ is less susceptible to reduction by the reactant mixture than $Rh(NO_3)_3/SiO_2$, resulting in higher hydroformylation selectivity. Increasing the reaction temperature from 393 to 513 K results in the reduction of $RhCl_3$ and $Rh(NO_3)_3$ to reduced Rh crystallites. Both catalysts remain active for hydroformylation and exhibit similar hydroformylation selectivities at 513 K. However, their selectivities for hydroformylation are significantly lower than those at 393 K. The low hydroformylation selectivity is related to the reduced Rh crystallite, which is highly active for hydrogenation.

INTRODUCTION

The nature of $Rh^+(CO)_2$, rhodium gem-dicarbonyl, on the supported Rh catalyst has been extensively studied for more than 3 decades (*1–17*). Spectroscopic studies of the adsorption of CO on the supported Rh catalyst demonstrated that the gem-dicarbonyl species exhibiting bands in the range of 2116–2090 cm^{-1} and 2048–2022 cm^{-1} are associated with isolated Rh^+ ions (*1–20*). Generation of $Rh^+(CO)_2$ on the oxide support can be achieved by (i) adsorption of CO on the oxidized or reduced Rh (*1–12*), (ii) exposure of supported $Rh_6(CO)_{16}$ and $Rh_4(CO)_{12}$ to oxygen (*13–15*), and (iii) the reaction of supported Rh salts such as chlorides and nitrates with CO and H_2O (*6, 14, 16, 17*). Most studies of $Rh^+(CO)_2$ have been confined to the vibrational spectroscopy of the gem-dicarbonyl and characterization of the state of rhodium which associates with the gem-dicarbonyl. Little work has been done on the activity of oxide-supported $Rh^+(CO)_2$ for catalytic reactions (*18, 19*).

One important industrial process that is catalyzed by Rh catalysts is olefin hydroformylation (*21–24*). The commercial hydroformylation catalyst consists of Rh carbonyls and complexes which are the most active and selective form of Rh catalysts. The reaction has also been found to occur on oxide- and zeolite-supported Rh (*25–28*), Rh-metal, and Rh oxides (*29–33*). A number of studies have suggested that the pathway for the hydroformylation on rhodium zeolite resembles that found in the homogeneous system (*26, 27*); Rh^+ sites on the oxide-supported Rh metal serve as the active site for the reaction (*29, 34–39*). These sugges-

[1] To whom correspondence should be addressed.

0021-9517/93 $5.00

tions are mainly derived from (i) the apparent similarity between the state of CO (or organic molecules) adsorbed on metal surfaces and the coordinated state of CO ligand (or organic fragments) bound to the metal atoms which form the mononuclear or polynuclear complexes and (ii) the ostensible analogy between the well-defined organometallic reaction steps and the elementary steps on heterogeneous catalyst surfaces (*40–48*).

This paper reports the results of a study on the interactions of C_2H_4 and H_2 with $Rh^+(CO)_2/SiO_2$ and CO adsorbed on Rh chloride and Rh nitrate and the activity of these catatlysts for hydroformylation (the Oxo reaction). The nature of $Rh^+(CO)_2$ and CO adsorbed on $RhCl_3/SiO_2$ and $Rh(NO_3)_3/SiO_2$ was characterized by temperature-programmed decomposition. The reactivity of various adsorbed CO species for propionaldehyde formation was determined by *in situ* infrared studies of the reaction of adsorbed CO with C_2H_4/H_2. *In situ* infrared studies of ethylene hydroformylation were carried out with the catalyst precursors containing $Rh^+(CO)_2$ and CO adsorbed on Rh ions ranging from the condition in which $Rh^+(CO)_2$ can stay intact to that in which $Rh^+(CO)_2$ can be decomposed to Rh metal. A correlation between the infrared intensity of various forms of adsorbed CO and hydroformylation activity under reaction conditions provides insight into the role of $Rh^+(CO)_2$ in the hydroformylation reaction. The types of adsorbed CO are closely related to the states of Rh (*1–17*). The results of this study shed light on the nature of active sites for hydroformylation on the heterogeneous Rh catalyst.

EXPERIMENTAL

Supported rhodium chloride and nitrate samples containing 3 wt% Rh were prepared by impregnation of silica (large pore, Strem Chemicals) with aqueous solutions of $RhCl_3 \cdot XH_2O$ (42.5% Rh) and $Rh(NO_3)_3 \cdot 2H_2O$ (32% Rh) (Alfa), respectively. Each gram of silica was impregnated with 1 cm^3 of solution. The resulting silica-supported Rh chloride and nitrate were dried in air at 313 K for 24 h and were pressed into self-supporting disks (10 mm in diameter, 1 mm in thickness, and 25 mg). The disk was placed in an infrared (IR) cell for infrared studies of CO adsorption and reactions. Transmission infrared spectra were obtained by a Nicolet 5SXC Fourier transform infrared spectrometer at a resolution of 4 cm^{-1}. The spectrum of the catalyst disk before admission of adsorbate was used as a background spectrum.

$Rh^+(CO)_2/SiO_2$ was prepared by chemisorption of CO on the $RhCl_3 \cdot XH_2O/SiO_2$ and $Rh(NO_3)_3 \cdot XH_2O/SiO_2$ at 298 K. The amount of H_2O in the catalyst samples prior to CO chemisorption was not determined. CO chemisorption led to carbonylation of $RhCl_3 \cdot XH_2O$ and $Rh(NO_3)_3 \cdot XH_2O$ according to the following reactions (*28, 50*):

$$Rh^{3+} + 3\,CO + H_2O \rightarrow Rh^+(CO)_2 + 2\,H^+ + CO_2$$

$$Rh^{3+} + 3\,CO + OH^- \rightarrow Rh^+(CO)_2 + H^+ + CO_2.$$

Due to the vague change in the IR spectra of OH^- and H_2O during carbonylation, the extent of the contribution of the above reactions to the formation of gem-dicarbonyl cannot be accurately determined from infrared spectroscopy. Carbonylation produced not only $Rh^+(CO)_2$ but also linear CO species adsorbed on Rh ions. It also led to a change in the apparent color of the $RhCl_3/SiO_2$ sample from pink to pale orange and that of $Rh(NO_3)_3/SiO_2$ from pale yellow to pale orange.

Temperature-programmed decomposition (TPDE) was used to determine the thermal stability of adsorbed CO and $Rh^+(CO)_2$ species on the catalyst. TPDE was conducted in a high-temperature IR cell which is capable of operating up to 723 K and 6 MPa. The pathlength for the infrared beam in the cell is slightly less than 2.7 mm and the net reactor volume is 0.21 cm^3. After the carbonylation of Rh chloride and nitrate in the IR cell, the catalyst was heated in flowing helium at 60 cm^3/min from 303 to 673 K

at a rate of 15 K/min. The composition of the effluent from the IR cell during TPDE was determined by a Balzer QMG-112 mass spectrometer.

The reaction of C_2H_4 and H_2 with $Rh^+(CO)_2$ and CO adsorbed on the catalyst was performed in a low temperature IR cell (*49*). The path length for the infrared beam in the cell is slightly less than 2 mm and the net reactor volume is 0.2 cm^3. The reactor cell can be used up to pressures of 6 MPa in a temperature range of 293 to 563 K. Following carbonylation of Rh chloride and nitrate and removal of gaseous CO by flushing the sample with N_2, the sample containing adsorbed CO was exposed to a mixture of C_2H_4 and H_2 (C_2H_4:H_2 = 1:1) at approximately 0.1 MPa and 298 K. The change in the IR intensity of the adsorbed species during TPDE and reactions was measured by the infrared spectrometer.

Steady-state ethylene hydroformylation (CO:H_2:C_2H_4 = 1:1:1) was carried out in the same IR cell at 393–513 K and 0.1–1 MPa. H_2 (UHP, 99.999%), CO (CP, 99.0%), He (UHP, 99.999%), C_2H_4 (CP, 99.5%) were purified by passing through a trap of liquid nitrogen before use. The reaction products were analyzed by an HP-5890A gas chromatograph with a 6-ft Poropak PS in series with a 6-ft Poropak QS column. IR spectra were taken during the entire course of reaction studies. The loading of Rh before and after the TPDE and steady-state reaction studies was determined by a Philips PV 9550 X-ray fluorescence spectrometer.

RESULTS

Temperature-Programmed Decomposition (TPDE)

The infrared spectra taken during temperature-programmed decomposition of $Rh^+(CO)_2$ and adsorbed CO on $RhCl_3/SiO_2$ is shown in Fig. 1. Prior to the TPDE study, infrared spectra for CO adsorbed on $RhCl_3/SiO_2$ at 303 K showed three major bands at 2145, 2102, and 2036 cm^{-1}. These bands were observed following exposure of $RhCl_3/SiO_2$ to 1 MPa of CO for 30 min at 303 K and

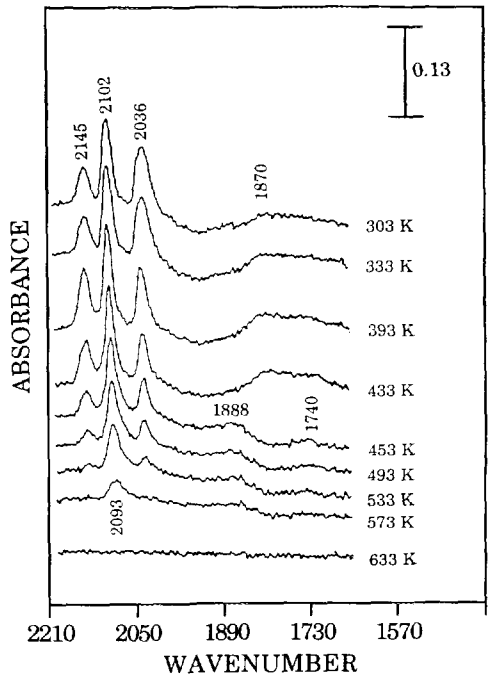

FIG. 1. Infrared spectra of $Rh^+(CO)_2$ and CO adsorbed on $RhCl_3/SiO_2$ during TPDE.

flushing the sample with nitrogen. These IR bands closely match those resulting from exposure of $RhCl_3/SiO_2$ to CO at 0.08–0.1 MPa and 323 K for 0.5–1 h (*13, 16, 17*). The intense bands at 2102 and 2036 cm^{-1} can be tentatively assigned to symmetric and asymmetric stretching of $Rh^+(CO)_2$, respectively. The high frequency band at 2145 cm^{-1} has been attributed to linear CO adsorbed on Rh^{+3}; the intensity of the band appears to depend upon details of treatments (*6, 13, 16–18*). The weak band at 1870 cm^{-1} is assigned to bridge-bonded CO.

The major gas phase products resulting from TPDE are CO and CO_2, whose TPDE profiles are shown in Fig. 2A; the variation of the IR absorbance of the three major bands as a function of temperature are plotted in Fig. 2B. Both CO and CO_2 were immediately observed as temperature increased from 303 K. The high base-line concentration of CO at the onset of TPDE is due to the nonlinear increase of the reactor temper-

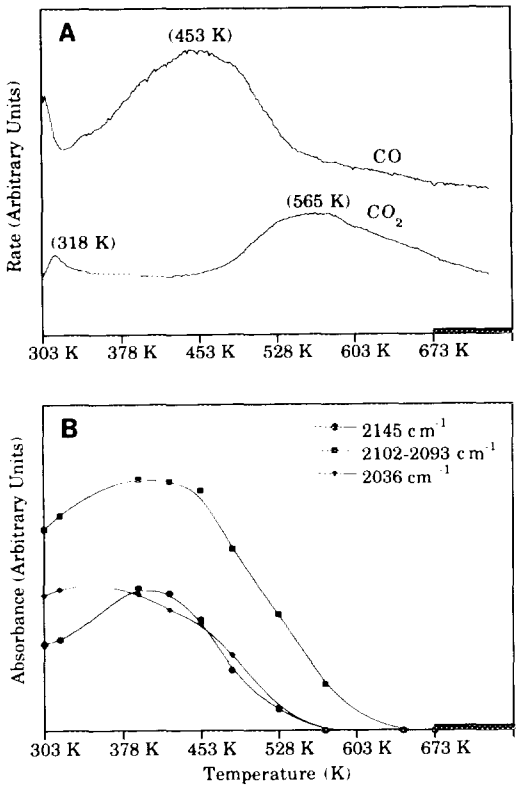

FIG. 2. (A) CO and CO_2 profiles during TPDE; (B) variation of absorbance of IR bands with temperature.

ature between 303 and 323 K. Both 2145- and 2102-cm^{-1} bands increased in intensity with temperature to 393 K. The reason for the slightly increased intensity with temperature remains unclear. Further increase in temperature caused decreases in the intensity of all the bands at about the same rate. The peak temperature for CO occurred at 453 K where a substantial decrease in the intensity of all the IR bands began. The peak temperature for CO_2 was observed at 565 K where both 2145- and 2036-cm^{-1} bands were almost completely removed from the surface of the catalyst. CO_2 may be formed by either (i) CO disproportionation [$2CO \rightarrow CO_2 + C$] or (ii) the reduction of Rh^+ by oxidation of a CO ligand (*51*) [$2Rh^+(CO)_2 + O^{-2} \rightarrow 2Rh\text{-}CO + CO_2 + 2CO$ (*12*), where O^{-2} is an oxygen of a surface oxide]. The occurrence of the latter would lead to the simultaneous formation of CO and CO_2. The significant difference in CO and CO_2 peak temperatures indicates that CO disproportionation is the dominant pathway for the formation of CO_2. CO disproportionation has also been proposed to be the major pathway for the formation of CO_2 during TPDE of oxide-supported metal carbonyls (*52*).

Upon reaching 573 K, both the 2145- and 2036-cm^{-1} bands were completely removed, leaving a residual CO species exhibiting a band at 2093 cm^{-1}. This band may be assigned to a linear (terminal) CO adsorbed on a Rh^+ site. This is consistent with a number of studies which have shown that isolated Rh^+ can chemisorb CO in both the gem-dicarbonyl and linear forms (*6, 53,54*). The linear CO adsorbed on a Rh^+ site exhibited an IR band in the 2080–2100 cm^{-1} range (*6, 54*). However, the distinction between Rh^+ sites that adsorb linear CO and Rh^+ sites that adsorb gem-dicarbonyl remains unclear. The 2102–2105 cm^{-1} band which was previously assigned to the symmetric stretching vibration of gem-dicarbonyl is apparently due to the combination of the symmetric vibration of the gem-dicarbonyl and the vibration of a linear CO species on a Rh^+ site. Such a combination yields an unusually high intensity ratio of the 2102-cm^{-1} to the 2036-cm^{-1} band.

Figure 3 shows the infrared spectra taken during temperature-programmed decomposition of $Rh^+(CO)_2$ and adsorbed CO on $Rh(NO_3)_3/SiO_2$. The adsorption of CO on $Rh(NO_3)_3/SiO_2$ at 303 K produced four bands at 2104, 2091, 2036 cm^{-1}, and a shoulder at 2083 cm^{-1}. The former three bands agree well with those reported by Keyes and Watters (*16, 17*). The 2091- and 2036-cm^{-1} bands may be attributed to a gem-dicarbonyl. The 2104-cm^{-1} band may be assigned to a linear CO adsorbed on either Rh^+ or Rh^{+2} sites; the assignment remains inconclusive. The shoulder band at 2083 cm^{-1} could be due to CO adsorbed on a partially oxidized Rh; this CO species completely desorbed at temperature below 393 K.

Figure 4A shows the CO peak tempera-

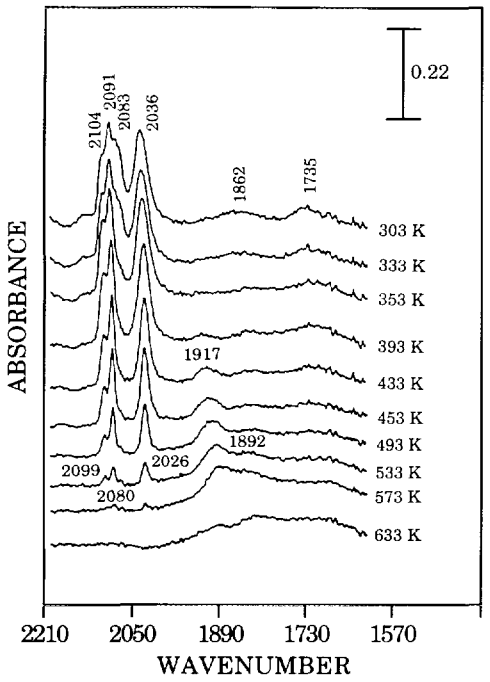

FIG. 3. Infrared spectra of $Rh^+(CO)_2$ and CO adsorbed on $Rh(NO_3)_3/SiO_2$ during TPDE.

ture at 335 K and CO_2 peak temperature at 393 K where substantial decreases in absorbance of the 2104-, 2091-, and 2036-cm^{-1} bands began. Figure 4B shows the variation in IR absorbance of adsorbed CO species as a function of temperature. Although CO desorption and disproportionation occurred at lower temperatures on $Rh(NO_3)_3/SiO_2$ than it did on $RhCl_3/SiO_2$, the temperature for the complete decomposition of $Rh^+(CO)_2$ was higher on $Rh(NO_3)_3/SiO_2$ than on $RhCl_3/SiO_2$. In addition to CO desorption and disproportionation, XRF analysis before and after the TPDE revealed that the Rh loading decreased from 3 to 2 wt% on $RhCl_3/SiO_2$, and from 3 to 2.7 wt% on $Rh(NO_3)_3/SiO_2$.

Since CO disproportionation is considered to be the major pathway for the formation of CO_2, each CO_2 molecule is produced by two adsorbed CO. The total amount of CO adsorbed prior to TPDE, listed in Table 1, was estimated by (i) summation of the number of CO desorbed and two times the number of CO_2 produced during TPDE and (ii) adjustment of the resulting value for Rh lost during TPDE assuming that the Rh dispersion remains constant. Although both catalysts contain the same amount of Rh salt whose crystallite size is determined to be less than 35Å by X-ray diffraction line-broadening, $Rh(NO_3)_3/SiO_2$ showed a higher CO chemisorption capability than $RhCl_3/SiO_2$.

Interactions of C_2H_4/H_2 with $Rh^+(CO)_2$ and CO Adsorbed on Silica-Supported Rh Chloride and Nitrate

Figure 5 shows the IR spectra for the reaction of C_2H_4/H_2 with CO adsorbed on $RhCl_3/SiO_2$ at 298 K. The initial spectrum prior to the admission of C_2H_4/H_2 to the

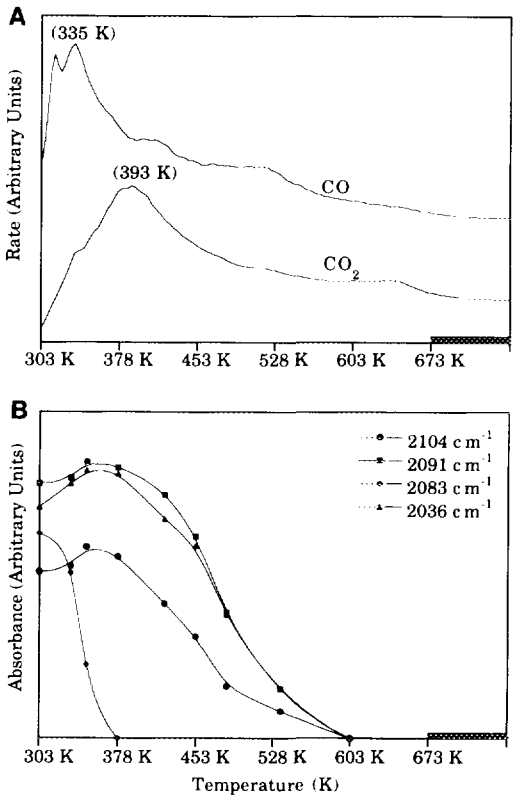

FIG. 4. (A) CO and CO_2 profiles during TPDE; (B) variation of absorbance of IR bands with temperature.

TABLE 1

Ethylene Hydroformylation over $RhCl_3/SiO_2$ and $Rh(NO_3)_3/SiO_2$ at 393 K and 1 MPa

Reaction time (min)	Rate of C_2H_4 conversion (mol/kg h)	TOF ($sec^{-1} \times 10^3$)	Selectivity (mol%)			
			CH_4	C_2H_6	C_2H_5CHO	C_3HC
		Catalyst: $RhCl_3/SiO_2$				
90	0.09	1.16	12.8	52.0	35.2	0.0
150	0.20	2.50	18.7	49.3	32.0	0.0
180	0.35	3.83	14.1	37.9	48.0	0.0
220	0.39	4.88	13.5	34.9	51.6	0.0
250	0.38	4.75	14.0	35.1	50.9	0.0
280	0.36	4.50	10.8	34.8	54.4	0.0
		Catalyst: $Rh(NO_3)_3/SiO_2$				
30	0.27	0.38	14.0	59.9	25.8	0.3
90	0.29	0.41	13.5	58.9	26.8	0.8
120	0.27	0.38	13.0	55.0	31.3	0.7
180	0.29	0.41	12.4	50.7	36.2	0.7
215	0.27	0.38	12.8	52.6	33.9	0.7

Amount of CO(ads) on $RhCl_3/SiO_2$ before TPDE and reaction
$= 83.13 \times 10^{-6}$ mol/gm cat

Amount of CO(ads) on $RhCl_3/SiO_2$ (corrected to Rh loss during the reaction)
$= 22.16 \times 10^{-6}$ mol/gm cat

Amount of CO(ads) on $Rh(NO_3)_3/SiO_2$ before TPDE and reaction
$= 197.1 \times 10^{-6}$ mol/gm cat

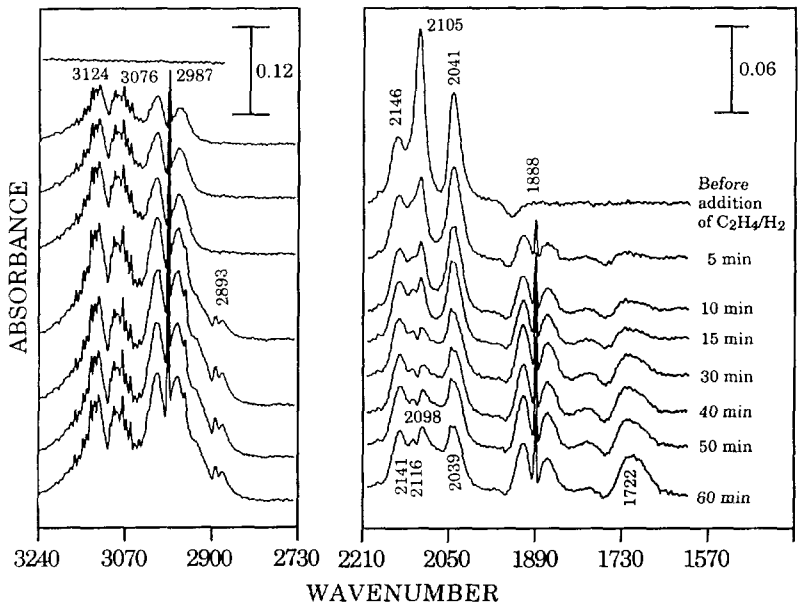

FIG.. 5. Infrared spectra for the reaction of C_2H_4/H_2 with $Rh^+(CO)_2$ and CO adsorbed on $RhCl_3/SiO_2$ at 298 K.

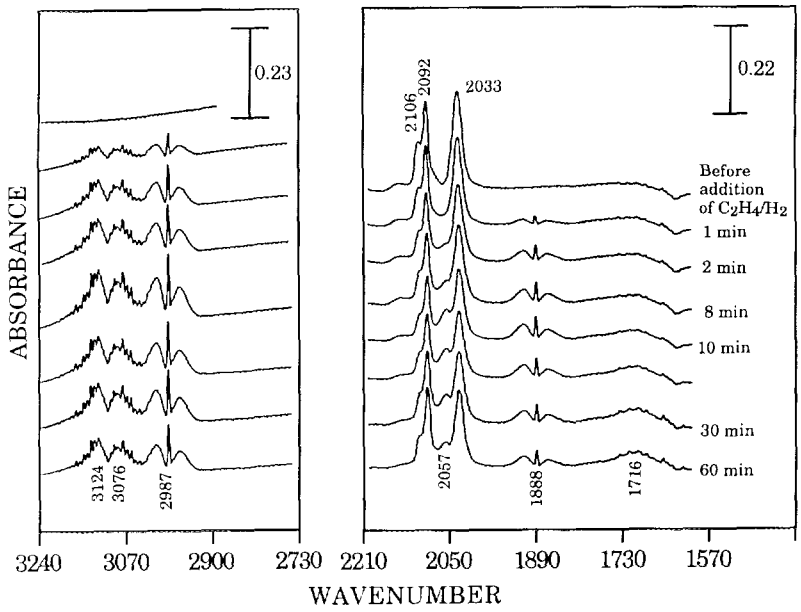

FIG. 6. Infrared spectra for the reaction of C_2H_4/H_2 with $Rh^+(CO)_2$ and CO adsorbed on $Rh(NO_3)_3/SiO_2$ at 298 K.

IR cell shows the IR band for CO adsorbed on Rh^{+3} at 2146 cm^{-1} and the gem-dicarbonyl bands at 2105 and 2041 cm^{-1}, which are similar to those at 303 K shown in Fig. 1. Exposure of CO adsorbed on $RhCl_3/SiO_2$ to 0.1 MPa of a C_2H_4/H_2 mixture at 298 K led to the following spectroscopic changes: (i) an initial, rapid decrease in the intensity and a downward shift of the 2105-cm^{-1} band, (ii) a gradual decrease in the intensity of the band at 2041 cm^{-1} which then split into two bands at 2045 and 2039 cm^{-1}, (iii) an increase in the intensity of the propionaldehyde band at 1722 cm^{-1}, (iv) an emergence of C–H stretching vibration of ethane at 2850-3000 cm^{-1} after 15 min of reaction, and (v) a slight change in intensity and wavenumber for the band at 2146 cm^{-1}. Gaseous ethylene shows IR bands at 1850–1900 and 2900–3200 cm^{-1}. No obvious change in the spectra was observed after 60 min of reaction as the reaction appeared to reach equilibrium.

The initial decrease in the intensity of the band at 2105 cm^{-1} correlated to the increase in the intensity of the propionaldehyde band at 1722 cm^{-1}. Due to the overlapping of the symmetric vibration of gem-dicarbonyl with the vibration of linear CO on Rh^+ at 2105 cm^{-1}, the contribution of the gem-dicarbonyl to the formation of propionaldehyde has to be determined from the decrease in the intensity of the asymmetric vibrational band at 2041 cm^{-1}. A gradual decrease in the intensity of the asymmetric vibration band at 2041 cm^{-1}, as well as a rapid initial decrease in the intensity and a downward shift of the band at 2105 cm^{-1}, suggests that the involvement of linear CO on Rh^+ sites in the formation of propionaldehyde is significantly more than that of the gem-dicarbonyl during the first 15 min of the reaction.

Figure 6 shows the spectral development for the reaction of C_2H_4 and H_2 with CO on $Rh(NO_3)_3/SiO_2$ at 298 K. The initial spectrum prior to the reaction consisted of the bands at 2106, 2092, and 2033 cm^{-1}, which are similar to those shown in Fig. 3. The intensity of the bands at 2092, 2106, and 2033 cm^{-1} showed an initial decrease sub-

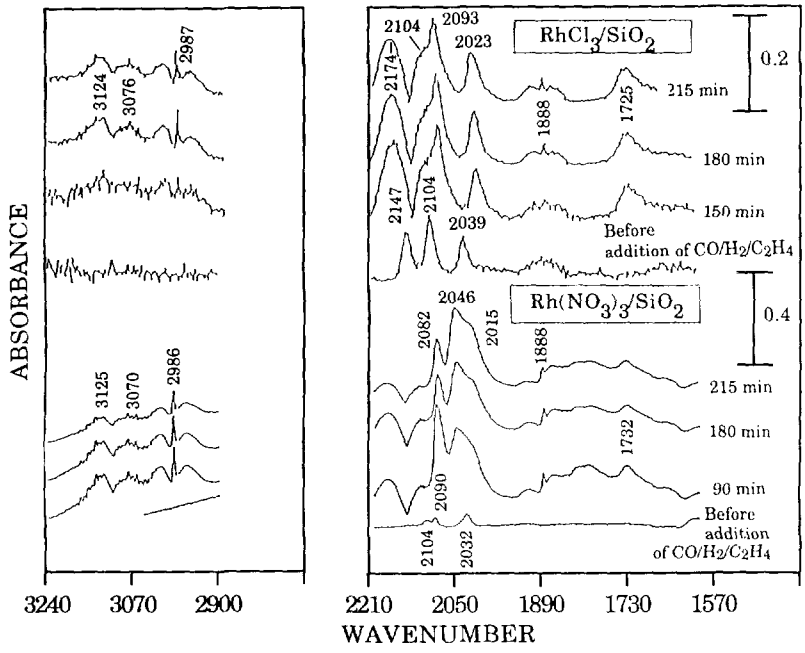

FIG. 7. Infrared spectra for ethylene hydroformylation on $RhCl_3/SiO_2$ and $Rh(NO_3)_3/SiO_2$ at 393 K and 1 MPa.

stantially and a gradual constant decrease with reaction time; the intensity of the propionaldehyde band at 1716 cm^{-1} increased slowly with reaction time. The rate of increase in the intensity of propionaldehyde band is significantly lower on $Rh(NO_3)_3/SiO_2$ than on $RhCl_3/SiO_2$. The development of the 2057 cm^{-1} band after 2 min of reaction indicates that a part of the surface has been reduced to the Rh^0 state that adsorbs linear CO.

Steady-State Ethylene Hydroformylation

The IR spectra for ethylene hydroformylation on $RhCl_3/SiO_2$ and $Rh(NO_3)_3/SiO_2$ at 393 K and 1 MPa are shown in Fig. 7. Exposure of CO adsorbed on $RhCl_3/SiO_2$ to a steady-state flow of $CO/H_2/C_2H_4$ gave rise to the propionaldehyde band at 1725 cm^{-1} and weak ethane bands in the 2850–3000 cm^{-1} region. The gem-dicarbonyl bands shifted from 2104 and 2039 cm^{-1} to 2093 and 2023 cm^{-1}, respectively. It should be noted that exposure of gem-dicarbonyl to H_2 may lead to the reduction of Rh^+ to Rh^0, resulting in the formation of adsorbed CO on Rh^0 sites and HCO (carbonyl hydride). The latter species displays an IR band in the 2027–2040 cm^{-1} range which overlaps with the asymmetric vibration (the low-frequency band) of gem-dicarbonyl. The formation of carbonyl hydride would change the contour of the low-frequency band of the gem-dicarbonyl. The formation of carbonyl hydride can be ruled out because both 2023-cm^{-1} and 2039-cm^{-1} bands have similar contours.

There was no obvious change in the IR spectra during the entire course of the reaction. Table 1 presents the rates of C_2H_4 conversion and selectivity corresponding to the IR spectra shown in Fig. 7. Ethane and propionaldehyde were the major products; methane and C_3 hydrocarbons were the minor products. The rate of C_2H_4 conversion and product selectivity showed an initial variation and then remained constant during

5 h of reaction; the XRF analysis of the catalyst after the reaction study showed that the Rh loading decreased from 3 to 0.8 wt%. The stable rate of product formation after an initial variation suggests that most of the Rh loss occurred during the initial stages of the reaction. The concentration of the Rh species in the effluent of the reactor was below the detection limit of our infrared and mass spectrometers. The forms of the lost Rh species in the effluent stream remains unclear.

TOF (turnover frequency) in Table 1 was calculated by dividing rate by the number of CO molecules adsorbed (adjusted for the percentage of Rh loss). Although a similar approach has been used to estimate TOF for hydroformylation over Rh/SiO_2 catalysts (*54*), it should be noted that the ratio of CO/Rh surface atom depends on the way CO adsorbs. Lack of extinction coefficients (or absorption intensity) prohibits the use of TPDE and IR results to determine the number of Rh sites for linear CO and gem-dicarbonyl. TOF in Table 1 should be used cautiously and only for comparison.

Admission of a steady-state flow of $CO/H_2/C_2H_4$ to CO adsorbed on $Rh(NO_3)_3/SiO_2$ resulted in the formation of propionaldehyde and weak C_2H_6 bands which resemble those on $RhCl_3/SiO_2$ (Fig. 7). Selectivity data listed in Table 1 shows $Rh(NO_3)_3/SiO_2$ is more selective for ethylene hydrogenation than $RhCl_3/SiO_2$. The carbonyl band at 2082–2090 cm^{-1} first increased and then decreased gradually in intensity with reaction time. In contrast, the 2032-cm^{-1} band increased slightly in intensity and became a shoulder at 2032–2010 cm^{-1} as the 2046-cm^{-1} band slowly emerged as a dominant band in the final spectrum as shown in Fig. 7. The increase in intensity of the 2046-cm^{-1} band with reaction time is apparently due to the formation of Rh^0 during the reaction process. In spite of the distinct variation of CO bands at 2046 cm^{-1} with reaction time, the rate of C_2H_4 conversion and product selectivity remained essentially constant as the reaction proceeded.

Table 2 shows the rate of product formation and selectivity for ethylene hydroformylation on the $RhCl_3/SiO_2$ and the $Rh(NO_3)_3/SiO_2$ catalysts at 1 MPa and 513 K. The reaction produced C_2H_6 and propionaldehyde as major products. The rate of C_2H_4 conversion and product selectivity remain essentially constant for the entire 3 h of reaction studies. $Rh(NO_3)_3/SiO_2$ exhibited higher activity for ethylene conversion and product formation than $RhCl_3/SiO_2$, but both catalysts showed similar selectivity. XRF analysis revealed that the Rh loading for $RhCl_3/SiO_2$ decreased from 3 to 1.9 wt%, while the Rh loading for $Rh(NO_3)_3/SiO_2$ remained constant during steady-state reaction studies. Figure 8 shows the IR spectra for the $CO/H_2/C_2H_4$ reaction on $RhCl_3/SiO_2$ and $Rh(NO_3)_3/SiO_2$, at 513 K and 1 MPa. The band near 2039 cm^{-1}, which may be assigned to a linear CO on Rh^0, increased in intensity with reaction time over $RhCl_3/SiO_2$. The broad band at 1890 cm^{-1} overlapping with the gaseous ethylene band corresponds to bridged CO. Reaction time has little influence on the propionaldehyde band at 1722 cm^{-1} and hydrocarbon (ethene and ethane) bands in the 2850–3200 cm^{-1} region.

The reaction on $Rh(NO_3)_3/SiO_2$ gave rise to a linear CO band at 2020 cm^{-1}, a propionaldehyde band at 1721 cm^{-1}, and hydrocarbon bands in the 2850–3200 cm^{-1} range. These bands were considerably more intense than those observed for the reaction on $RhCl_3/SiO_2$. The high intensity of linear and bridged CO bands for $Rh(NO_3)_3/SiO_2$ as compared to those for $RhCl_3/SiO_2$ indicates that the surface area of the metallic Rh crystallite is higher for the catalyst prepared from $Rh(NO_3)_3/SiO_2$ than that from $RhCl_3/SiO_2$.

DISCUSSION

Chemisorbed CO on $RhCl_3/SiO_2$ and $Rh(NO_3)_3/SiO_2$

Although both $RhCl_3/SiO_2$ and $Rh(NO_3)_3/SiO_2$ contain Rh^{+3} sites, adsorption of CO on Rh^{+3} associated with different anions results in the formation of linear CO and gem-

TABLE 2

Ethylene Hydroformylation over $RhCl_3/SiO_2$ and $Rh(NO_3)_3/SiO_2$ at 513 K and 1 MPa

Reaction time (min)	Rate of C_2H_4 conversion (mol/kg h)	TOF ($sec^{-1} \times 10^3$)	Selectivity (mol%)			
			CH_4	C_2H_6	C_2H_5CHO	C_3HC
		Catalyst: $RhCl_3/SiO_2$				
30	6.29	33.16	3.9	75.2	20.2	0.7
60	6.15	32.33	0.9	72.0	26.9	0.2
90	6.28	33.00	0.9	72.1	26.8	0.2
135	5.60	29.50	1.1	70.9	27.8	0.2
		Catalyst: $Rh(NO_3)_3/SiO_2$				
60	59.8	84.00	0.2	73.3	26.4	0.1
90	57.2	80.00	0.2	72.4	27.2	0.2
125	59.9	84.00	0.2	72.7	26.9	0.2

Amount of CO(ads) on $RhCl_3/SiO_2$ (corrected to Rh loss during the reaction) $= 52.64 \times 10^{-6}$ mol/gm cat

dicarbonyl which exhibit different vibrational frequencies and catalytic properties. The major forms of chemisorbed CO on $RhCl_3/SiO_2$ are the gem-dicarbonyl as well as the linear CO on Rh^{+3} and Rh^+ sites; the predominant forms of CO adsorbed on $Rh(NO_3)_3/SiO_2$ are gem-dicarbonyl and linear CO on Rh^+ (or Rh^{+2}) sites giving the

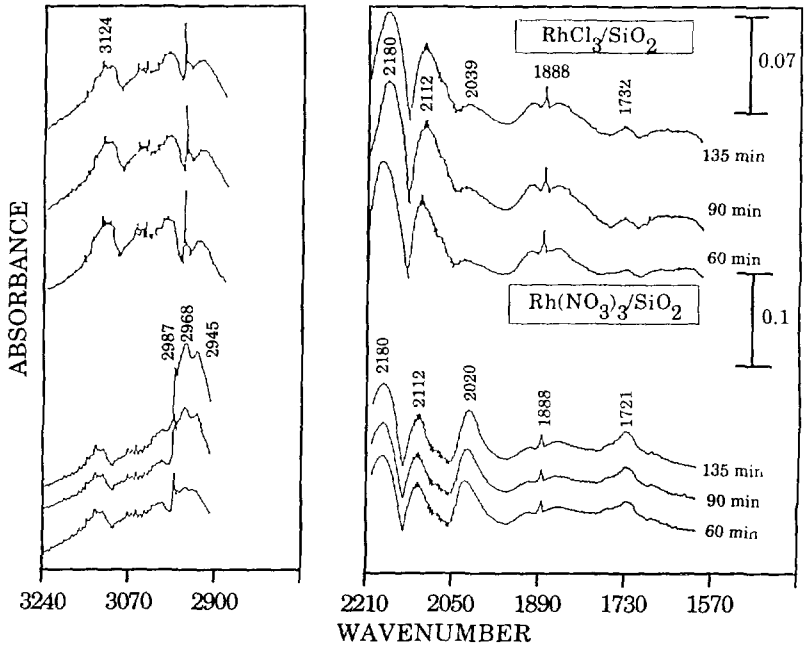

FIG. 8. Infrared spectra for ethylene hydroformylation on $RhCl_3/SiO_2$ and $Rh(NO_3)_3/SiO_2$ at 513 K and 1 MPa.

2105-cm^{-1} band. Keyes and Watters noted that the gem-dicarbonyl on $RhCl_3/SiO_2$ may be in the form of $[Rh(CO)_2Cl]_2$ physisorbed on the surface of SiO_2; the physisorbed carbonyl species can be readily extracted from the surface into pentane (*16, 17*). In fact, carbonylation of $RhCl_3$ with H_2O and CO is a standard approach for the preparation of $[Rh(CO)_2Cl]_2$ (*52, 55*). Due to its low boiling point (313–333 K), $[Rh(CO)_2Cl]_2$ can be evaporated and flushed out of the catalyst before being decomposed. However, mass and infrared spectroscopic analysis of the effluent of the TPDE reactor failed to identify $[Rh(CO)_2Cl]_2$. The concentration of $[Rh(CO)_2Cl]_2$ could be far below the detection limit of our mass and infrared spectrometers. XRF analysis revealed that the Rh loading for $RhCl_3/SiO_2$ decreased from 3 to 2 wt% while the Rh loading for $Rh(NO_3)_3/SiO_2$ only dropped to 2.7 wt% during TPDE studies.

It has been suggested that $Rh^+(CO)_2$ on $Rh(NO_3)_3/SiO_2$ may be in the form of $[Rh(CO)_2O_s]_2$ (where O_s is a surface oxide) which strongly interacts with the surface oxide; the species can not be removed from the surface by solvent extraction (*16, 17*). TPDE studies show that the temperature required for the complete removal of gem-dicarbonyl is higher on $Rh(NO_3)_3/SiO_2$ than on $RhCl_3/SiO_2$. Furthermore, most of the Rh species is retained on the surface of $Rh(NO_3)_3$ during TPDE studies.

The Formation of Propionaldehyde on $RhCl_3/SiO_2$ and $Rh(NO_3)_3/SiO_2$

The correlation between the decrease in the intensity of the 2105-cm^{-1} band and the increase in the intensity of propionaldehyde band indicates that the linear CO on Rh^+ sites displaying the 2105–2098 cm^{-1} band participates in the formation of propionaldehyde on $RhCl_3/SiO_2$. The involvement of gem-dicarbonyl in propionaldehyde formation is less than that of linear CO on Rh^+ as indicated by the slow attenuation of the asymmetric vibration band of gem-dicarbonyl (shown in Fig. 5). In contrast to the reaction on $RhCl_3/SiO_2$, the correlation between CO consumed and propionaldehyde formed on $Rh(NO_3)_3/SiO_2$ is not obvious enough to assign the type of adsorbed CO species responsible for the propionaldehyde formation. The adsorbed CO species on $Rh(NO_3)_3/SiO_2$ showed a significantly lower reactivity toward C_2H_4/H_2 than the linear CO on Rh^+ sites of $RhCl_3/SiO_2$ at 298 K.

The observation of involvement of linear CO on the Rh^+ site of $RhCl_3/SiO_2$ in the formation of propionaldehyde is in good agreement with our previous studies (*49*). Our previous studies on CO insertion on reduced and oxidized Rh/SiO_2 have shown that both single Rh^0 and Rh^+ sites that chemisorb linear CO are active for CO insertion leading to the formation of propionaldehyde from ethylene; Rh^+ sites appear to be more active than Rh^0 sites (*49*). The formation of propionaldehyde on supported Rh catalysts is proposed to involve three elementary steps: hydrogenation of adsorbed C_2H_4 to form adsorbed ethyl species, insertion of linearly adsorbed CO to form adsorbed acyl species, and then hydrogenation to produce propionaldehyde. Due to the transient nature of reaction intermediates, most of these proposed intermediates could not be identified by *in situ* infrared spectroscopy. Only stable adsorbed species were observed under hydroformylation conditions.

Steady-State Ethylene Hydroformylation on $RhCl_3/SiO_2$ and $Rh(NO_3)_3/SiO_2$

The dominant CO feature in steady-state ethylene hydroformylation on $RhCl_3/SiO_2$ at 393 K and 1 MPa is the gem-dicarbonyl exhibiting bands at 2093 and 2023 cm^{-1}, as shown in Fig. 7. By comparison of the infrared spectra of gem-dicarbonyl before and after exposure to C_2H_4/H_2 (Fig. 5) and $CO/H_2/C_2H_4$ reaction (Fig. 7), it is evident that gem-dicarbonyl in the atmosphere of $CO/H_2/C_2H_4$ exhibited lower wavenumbers than those in the absence of the reactant mixture. Physisorbed CO has been observed to shift the vibrational frequency of

gem-dicarbonyl to lower wavenumbers at 80–320 K (*56*). The Rh carbonyl species exhibiting 2110- and 2044-cm^{-1} bands has been tentatively assigned to the $Rh^+(CO)_2(C_2H_4)$ (*57*) while the species displaying 2092- and 2025-cm^{-1} bands has been attributed to the $Rh^+(CO)_2H$ (*58*). No definite information is available to justify the existence of such species on the catalyst surface in the present study.

Although it remains unclear how coadsorbed ethylene and hydrogen affect the symmetric and asymmetric vibration of the gem-dicarbonyl, the presence of the gem-dicarbonyl in hydroformylation at 393 K and 1 MPa indicates that a significant fraction of the catalyst surface is in a Rh^+ state, and gem-dicarbonyl on $RhCl_3/SiO_2$ is stable under conditions of ethylene hydroformylation (393 K and 1 MPa). The present studies and previous studies of interactions of C_2H_4/H_2 with adsorbed CO have demonstrated that the terminal CO adsorbed on Rh^+ is involved in the reaction with C_2H_4/H_2 to form propionaldehyde at 298 K and 373 K; however, no clear band for the linear CO on Rh^+ sites can be observed in the high-pressure ethylene hydroformylation at 393 K due to the presence of intense gaseous CO bands. The presence of high-pressure CO in the reactant mixture could result in further adsorption of CO on the Rh^+ site which associates with a terminal carbon monoxide, $CO + Rh^+(CO) \rightarrow Rh^+(CO)_2$. The step has been suggested to be an intermediate step for the formation of $Rh^+(CO)_2$ from adsorption of CO on a highly dispersed Rh catalyst (*11*).

The major forms of adsorbed CO observed in steady-state ethylene hydroformylation on $Rh(NO_3)_3/SiO_2$ at 393 K and 1 MPa include a linear CO adsorbed on Rh^0 sites and gem-dicarbonyl. Evidence for the existence of carbonyl hydride remains inconclusive due to the presence of the linear CO band at 2046 cm^{-1} and the shoulder for asymmetric vibration of gem-dicarbonyl at 2015 cm^{-1}. The attenuation of the gem-dicarbonyl band and the growth of the band for the linear CO on Rh^0 sites indicate that a significant fraction of the $Rh(NO_3)_3/SiO_2$ surface was reduced to metallic Rh crystallites during the reaction. The reduction of $Rh(NO_3)_3/SiO_2$ to metallic crystallites in the reaction atmosphere occurred even at 298 K, as shown by the formation of linear CO on Rh^0 sites (shown in Fig. 6). The high-surface-area metallic Rh formed from $Rh(NO_3)_3/SiO_2$ is probably the reason why $Rh(NO_3)_3/SiO_2$ showed a considerably higher hydrogenation activity and selectivity than $RhCl_3/SiO_2$ at 393 K (Table 1).

Exposure of $RhCl_3/SiO_2$ and $Rh(NO_3)_3/SiO_2$ to a steady-state flow of $CO/H_2/C_2H_4$ at 513 K and 1 MPa gave rise to infrared absorption bands for the linear CO, bridge CO, adsorbed propionaldehyde, and C_2H_6. No infrared evidence for the gem-dicarbonyl was observed during ethylene hydroformylation at 513 K. Several infrared studies have also failed to detect the gem-dicarbonyl on the Rh^+ ion for $Zn–Rh/SiO_2$ and $Ag–Rh/SiO_2$ which showed high CO insertion selectivity (*59*, *60*). TPDE results in Figs. 1–4 have shown that only part of the gem-dicarbonyl on $RhCl_3$ and $Rh(NO_3)_3$ can survive under helium flow at 513 K. CO in the reactant mixture promotes agglomeration of isolated Rh^+ to metallic Rh crystallites converting gem-dicarbonyl to linear CO at temperatures above 448 K (*12*); and another reactant, hydrogen, further enhances the process. The presence of the linear and bridge CO and the absence of the gem-dicarbonyl show that a significant fraction of the catalyst surface has been reduced to metallic Rh crystallites. The observation of IR bands for linear CO on Rh^0 sites (Fig. 8) and similar selectivity for the formation of propionaldehyde on both $Rh(NO_3)_3$ and $RhCl_3$ catalysts at 513 and 1 MPa suggest that the reduced Rh sites catalyze hydroformylation. This observation is in agreement with a previous proposition that the single Rh^0 sites that chemisorb linear CO are active for hydroformylation (*49*).

CONCLUSIONS

The origin of the difference in vibrational frequencies and properties of gem-dicarbonyl and linear CO on $RhCl_3/SiO_2$ and $Rh(NO_3)_3/SiO_2$ catalysts may be related to the anions associated with Rh species. CO adsorption on $RhCl_3/SiO_2$ produced $Rh^+(CO)_2$, linear CO on Rh^+ sites, and linear CO on Rh^{+3} sites; CO adsorption on $Rh(NO_3)_3/SiO_2$ formed $Rh^+(CO)_2$ and linear CO on Rh^+ (or Rh^{+2}) sites. Thermal stability of these various CO species decreased in the following order: linear CO on Rh^+ of $RhCl_3/SiO_2$ > $Rh^+(CO)_2$ on $Rh(NO_3)_3/SiO_2$ > $Rh^+(CO)_2$ and linear CO on Rh^{+3} on $RhCl_3/SiO_2$. Linear CO on Rh^+ sites is more active than $Rh^+(CO)_2$ on either $Rh(NO_3)_3/SiO_2$ or $RhCl_3/SiO_2$ catalysts at 298 K toward C_2H_4 and H_2 leading to the formation of propionaldehyde.

Under ethylene hydroformylation condition ($CO/H_2/C_2H_4$, 393 K and 1 MPa), the dominant CO species is gem-dicarbonyl on $RhCl_3/SiO_2$, indicating that most surface Rh is in the Rh^+ state while the major forms of CO on $Rh(NO_3)_3/SiO_2$ are linear CO on Rh^0 sites and gem-dicarbonyl. $Rh(NO_3)_3/SiO_2$ is more susceptible to reduction by the reactant mixture than $RhCl_3/SiO_2$, resulting in higher hydrogenation selectivity. Increasing the reaction temperature from 393 to 513 K led to the emergence of linear CO on Rh crystallites which were reduced from $RhCl_3$ and $Rh(NO_3)_3$. Although both catalysts remain active for hydroformylation at 513 K, their selectivities are significantly lower than those at 393 K. The low hydroformylation selectivity appears to be associated with the reduced Rh crystallites which are highly active for hydrogenation.

ACKNOWLEDGMENTS

Funding for this research was provided by the U.S. Department of Energy under Grant DE-FG22-87PC79923. The authors thank Mr. S. Debnath for the XRF analysis.

REFERENCES

1. Yang, A. C., and Garland, C. W., *J. Phys. Chem.* **61,** 1504 (1957).
2. Yates, J. T., Jr., Duncan, T. M., Worley, S. D., and Vaughn, R. W., *J. Chem. Phys.* **70,** 1219 (1979).
3. Yates, J. T., Jr., Duncan, T. M., and Vaughn, R. W., *J. Chem. Phys.* **71,** 3908 (1979).
4. Antoniewicz, P. R., Cavanagh, R. R., and Yates, J. T., Jr., *J. Chem. Phys.* **73,** 3456 (1980).
5. Cavanagh, R. R., and Yates, J. T., Jr., *J. Chem. Phys.* **74,** 4150 (1981).
6. Rice, C. A., Worley, S. D., Curtis, C. W., Guin, J. A., and Tarrer, A. R., *J. Chem. Phys.* **74,** 6487 (1981).
7. Worley, S. D., Rice, C. A., Mattson, G. A., Curtis, C. W., Guin, J. A., and Tarrer, A. R., *J. Phys. Chem.* **86,** 2714 (1982).
8. Worley, S. D., Rice, C. A., Mattson, G. A., Curtis, C. W., Guin, J. A., and Tarrer, A. R., *J. Chem. Phys.* **76,** 20 (1982).
9. van't Blik, H. F. J., Van Zon, J. B. A. D., Huizinga, T., Vis, J. C., Koningsberger, D. C., and Prins, R., *J. Phys. Chem.* **87,** 2264 (1983).
10. Basu, P., Panayotov, D., and Yates, J. T., Jr., *J. Phys. Chem.* **91,** 3133 (1987).
11. Basu, P., Panayotov, D., and Yates, J. T., Jr., *J. Am. Chem. Soc.* **110,** 2074 (1988).
12. Solymosi, F., and Pasztor, M., *J. Phys. Chem.* **89,** 4789 (1985).
13. Bilhou, J. L., Bilhou-Bougnol, V., Graydon, W. F., Basset, J. M., Smith, A. K., Zanderighi, G. M., Ugo, R., *J. Organomet. Chem.* **153,** 73 (1978).
14. Smith, A. K., Hughes, F., Theolier, A., Basset, J. M., Ugo, R., Zanderighi, G. M., Bilhou, J. L., Bilhou-Bougnol, V., and Graydon, W. F., *Inorg. Chem.* **18,** 3104 (1979).
15. Theolier, A., Smith, A. K., Leconte, M., Basset, J. M., Zanderighi, G. M., Psaro, R., and Ugo, R., *J. Orgnomet. Chem.* **191,** 415 (1980).
16. Keyes, M. P., and Watters, K. L., *J. Catal.* **100,** 477 (1986).
17. Keyes, M. P., and Watters, K. L., *J. Catal.* **110,** 96 (1988).
18. Scurrell, M. S., *J. Mol. Catal.* **10,** 57 (1981).
19. Primet, M., and Garbowski, E., *Chem. Phys. Lett.* **72**(3), 472 (1980).
20. Shannon, R. D., Vederine, J. C., Naccache, C., and Lefebvre, F., *J. Catal.* **88,** 431, (1984).
21. Pino, P., Piacenti, F., and Bianchi, M., *in* "Organic Synthesis via Metal Carbonyls" (I. Wender and P. Pino, Eds.), Vol. 2, p. 43. Wiley, New York, 1977.
22. Cornils, B., *in* "New Synthesis with Carbon Monoxide" (J. Fable, Ed.), p. 1. Springer-Verlag, Berlin–Heidelberg–New York, 1980.
23. Parshall, G. W., "Homogeneous Catalysis—The Applications and Chemistry of Catalysis by Soluble Transition Metal Complexes." Wiley, New York, 1981.

24. Masters, C., "Homogeneous Transition-Metal Catalysis—a General Art," p. 102. Chapman and Hall, New York and London, 1981.
25. Davis, M. E., Rode, E. J., Taylor, D., and Hanson, B. E., *J. Catal.* **86,** 67 (1984).
26. Rode, E. J., Davis, M. E., and Hanson, B. E., *J. Catal.* **96,** 563 (1985).
27. Rode, E. J., Davis, M. E., and Hanson, B. E., *J. Catal.* **96,** 574 (1985).
28. Takahashi, N., Mijin, A., Suematsu, H., Shinohara S., and Matsuoka, H., *J.Catal.* **117,** 348 (1989).
29. Watson, P. R., and Somorjai, G. A., *J. Catal.* **72,** 347 (1982).
30. Chuang, S. C., Tian, Y. H., Goodwin, J. G., Jr., and Wender, I., *J. Catal.* **96,** 396 (1985).
31. Chuang, S. C., and Pien, S. I., *J. Mol. Catal.* **55,** 12 (1989).
32. Ponec, V., *in* "Catalysis" (G. C. Bond and G. Webb, Eds.), p. 48. The Royal Society of Chemistry, London, 1982.
33. Gysling, H. J., Monnier, J. R., and Apai, G., *J. Catal.* **103,** 407 (1987).
34. Sachtler, W. M. H., and Ichikawa, M., *J. Phys. Chem.* **90,** 4752 (1986).
35. van den Berg, F. G. A., Ph.D. thesis. University of Leiden, The Netherlands, 1984.
36. Kawai, M., Uda, M., and Ichikawa, M., *J. Phys. Chem.* **89,** 1654 (1985).
37. Sachtler, W. M. H., *in* "Proceedings of the 8th International Congress on Catalysis, Berlin, 1984." Dechema, Frankfurt-am-Main, 1984.
38. van den Berg, F. G. A., Glezer, J. H. E., and Sachtler, W. M. H., *J. Catal.* **93,** 340 (1985).
39. Sachtler, W. M. H., Shriver, D. F., and Ichikawa, M., *J. Catal.* **99,** 513 (1986).
40. Henrici-Olivé, G., and Olivé, S., "The Chemistry of the Catalyzed Hydrogenation of Carbon Monoxide. "Springer-Verlag, New York, 1984.
41. Sheldon, R. A., "Chemicals from Synthesis Gas." D. Riedel., Boston, 1983.
42. Ugo, R., *Catal. Rev.* **11,** 225 (1975).
43. Muetterties, E. L., and Stein, J., *Chem. Rev.* **79,** 479 (1979).
44. Delmon, B., and Jannes, G. (Eds.), "Catalysis: Homogeneous and Heterogeneous." Elsevier, Amsterdam, 1975.
45. Halpern, J., *in* "Relation Between Homogeneous and Heterogeneous Catalysis" (J. M. Basset, Ed.), p. 28. CNRS Editions, Paris, 1978.
46. Ugo, R., and Psaro, R., *J. Mol. Catal.* **20,** 53 (1983).
47. Bradley, J. S., *in* "Metal Clusters" (M. Moskovits, Ed.), p. 105. Wiley, New York, 1986.
48. Gates, B. C., *in* "Metal Clusters" (M. Moskovits, Ed.), p. 283. Wiley, New York, 1986.
49. Chuang, S. S. C., and Pien, S. I., *J. Catal.* **135,** 618 (1992).
50. Conesa, J. C., Sainz, M. T., Soria, J., Munuera, G., Rives-Arnau, V., and Munoz, A., *J. Mol. Catal.* **17,** 231 (1982).
51. Lamb, H. H., Gates, B. C., and Knozinger, H., *Angew. Chem. Int. Ed. Engl.* **27,** 1127 (1988).
52. Knozinger, H., *in* "Metal Clusters in Catalysis" (B. C. Gates, L. Guczi, and H. Knozinger, Eds.) p. 259. Elsevier, Amsterdam–Oxford–New York–Tokyo, 1986.
53. Li, Y. E., and Gonzales, R. D., *J. Phys. Chem.* **92,** 1589 (1988).
54. Konishi, Y., Ichikawa, M., and Sachtler, W. M. H., *J. Phys. Chem.* **91,** 6286 (1987).
55. McCleverty, J. A., and Wilkinson, G., *Inorg. Synth.* **8,** 211 (1965).
56. Yates, J. T., Jr., and Haller, G. L., *J. Phys. Chem.* **88,** 4460 (1984).
57. Lefevre, F., and Ben Taarit, Y., *Nouv. J. Chim.* **8,** 387 (1984).
58. Yates, J. T., Worley, S. D., Duncan, T. M., and Vaughan, R. W., *J. Chem. Phys.* **70,** 1225 (1979).
59. Jen, H. W., Zheng, Y., Shriver, D. F., and Sachtler, W. M. H., *J. Catal.* **116,** 361 (1989).
60. Chuang, S. C., Pien, S. I., and Narayanan, R., *Appl. Catal.* **57,** 241 (1990).